Impact of Variable Atmospheric Water Vapor Content on AVHRR Data Corrections over Land

J. Cihlar, I. Tcherednichenko, R. Latifovic, Z. Li, and J. Chen

Abstract—**This paper explores the impact of the integrated water vapor content (IWV) in the atmospheric column on the corrections of optical satellite data over land. First, simulation runs were used to quantify the trends in red and near infrared parts of the electromagnetic spectrum. Second, advanced very high resolution radiometer (AVHRR) measurements obtained over Canada during the 1996 growing season, together with reanalyzed IWV content data, were employed to determine the actual impact of constant IWV values. Third, various options in characterizing IWV for atmospheric corrections of AVHRR composites were examined. It was found that 1) as expected, IWV affects near-infrared radiation substantially more than red, although the latter is also altered; 2) that additional, subtle interactions take place between IWV, radiance levels, and viewing geometry that influence the retrieved surface reflectance; 3) that spatial and temporal variation in IWV caused changes in the normalized difference vegetation index up to 7.5% in relative terms during the peak green period; and 4) that IWV varies so substantially that pixel- and date-specific values need to be used for the atmospheric correction of AVHRR data. At present, subdaily gridded IWV data sets from atmospheric data reanalysis projects are the only candidate source for such purpose.**

I. INTRODUCTION

IN REMOTE sensing applications concerned with land surface characteristics and processes, atmospheric interference is a serious limitation, particularly for sensors operating in the optical part of the electromagnetic spectrum. The scattering and absorption of solar radiation distorts the information embedded in the signal after its energy interacted with the target. For many application purposes, the fundamentals of the atmospheric attenuation process are well understood and have been embedded in radiative transfer models as well as in various computer codes [10]. The problem is in knowing the state of the atmosphere sufficiently well to be able to specify the atmospheric parameters upon which an accurate computation of atmospheric attenuation depends. Most important among these are aerosol optical depth, water content in the atmospheric column, and ozone. Because of an inadequate knowledge of these variables, constant values are often used [4] or the correction is omitted [7]. Of primary importance are water content and aerosols in the atmospheric column, which have a strong impact on the radiation reflected from the surface because of their variability and, in the case of water vapor, the position of water absorption bands. While aerosol concentrations are very important, previous and current

satellites offer minimal information upon which the estimation of optical depth over land could be effectively based. In this respect, launch of MODIS will provide a major improvement [12], but it will not be applicable to previous optical satellite data. The effect of ozone is weaker compared to that of water vapor, and there are alternative sources for its characterization [6], [15]. Previous studies concerned with the effect of integrated water vapor content (IWV) have employed actual radiosonde measurements [8] or satellite data in specific circumstances [17]. Unfortunately, such data are not available with a sufficient density to be of value for operational corrections of most existing satellite measurements over land. On the other hand, IWV is an output of numerical atmospheric models and this product could be used for such purpose.

In this paper, we are concerned with the impact of using constant IWV values in the processing of data from the advanced very high resolution radiometer (AVHRR) for biospheric studies at northern latitudes. In the past, the climatological value for summer, mid-latitude atmosphere (2.3 g/cm^2) was used to correct data for the Canadian landmass [2]. However, since the domain of interest spans the range of latitudes from < 45° to above 80° N, and the period of interest from April to October, a mid-latitude, mid-summer value, may not be adequate. The analysis consists of three parts. First, we evaluate the effect of variable IWV on individual AVHRR channels, as well as on the normalized difference vegetation index (NDVI) as an example of a transformation that diminishes various sources of noise [1]. Second, we examine the effect of fixed IWV value on the correction of actual AVHRR data over the Canadian landmass in different parts of the growing season. Third, we test various alternatives for specifying IWV distribution by taking into consideration both spatial and temporal fluctuations.

II. DATA AND METHODS

To assess the impact of varying IWV on the corrections of AVHRR channels 1 (C1, 0.57–0.70 μm) and 2 (C2, 0.71–0.98 μm), we carried out simulations using $6S$ [18] in the reverse mode. This algorithm permits calculation of spectral reflectance at the surface level for a given combination of top- of-the-atmosphere (TOA) radiance, view zenith angle (VZA), solar zenith angle (SZA), relative azimuth angle (RA), IWV, and aerosol optical depth. Calculations were made for all combinations of: two SZAs (40°, 55°), five VZAs (0°, 15°,···, 45°), five TOA radiances (20, 40, ···, 100 Wm^{-2}sr^{-1} μm^{-1}), and eight IWV values (0, 0.5,···, 3.0 g/cm^2). These ranges were chosen to represent the typical range of values found in seasonal AVHRR composites at northern latitudes. The RA value was 0° (backscatter), aerosol optical depth

0.05 (continental type), and Lambertian surface reflectance distribution function was assumed.

The AVHRR radiance data employed in this study were NOAA-14 (afternoon pass), ten-day composite images for three periods in 1996: May 1–10, July 21–31, and October 21–31. The GEOCOMP system [18] was used to process the AVHRR data. The daily data over Canada were geometrically corrected, registered to Lambert Conformal Conic (LCC) Projection; standard parallels 49° and 77° N, reference meridian 95° W), resampled at 1 km pixel size, and composited into ten or eleven-day, nominally cloud-free images using the maximum NDVI value as the selection criterion. GEOCOMP produces composites of five AVHRR channels, three angle channels (VZA, SZA, RA), NDVI, and date of imaging. Cihlar *et al.* [2], [3] provide more detail on the processing methodology. For the subsequent processing discussed in this paper, the composites were subsampled by selecting every sixth line and sixth pixel, thus obtaining an image with 246 521 land pixels.

Based on the above input AVHRR image data, atmospheric corrections were computed using the SMAC algorithm [16]. We assumed that for the range of parameters employed, the difference between the $6S$ and SMAC was negligible [16]. Two computations were made for each of AVHRR channels 1 and 2, both using 0.35 cm-atm for ozone and 0.05 for atmospheric optical depth at 550 nm. In the first computation, a constant IWV $= 2.3$ g/cm^2 was used. In the second case, IWV varied with the pixel and the acquisition date. Pixel-specific IWV values were obtained for this purpose from the NCEP/NCAR global reanalysis data set [9]. Based on a dynamic atmospheric models, this data set provides estimates of several parameters four times per day, at a spatial resolution of $1° \times 1°$ in geographic coordinates (platte carree) for the period 1987 to 1996. For our study, we used the value for 1800 GMT after ascertaining that the IWV difference compared to the 1200 GMT time period was small. The original data were reprojected into the LCC, interpolated to AVHRR composite pixels using bilinear interpolation, and used to prepare several data layers as described below. The intent was to investigate the effectiveness of various composite IWV data sets, differing by the ease of implementation, as a substitute for the fixed IWV value in atmospheric corrections of AVHRR data.

After computing the C1, C2, and NDVI values with the two IWV (IWV$_{const}$ $= 2.3$ g/cm^2 and pixel- and date-specific, termed "IWV$_{true}$" hereinafter), the overall mean (AV), average difference (AVD) and relative change (RC, in percent) were calculated as follows:

$$AV(j, k, m)$$
$$= \frac{1}{NP} \sum_{i=1}^{NP} C(i, j, k, PW_m), \qquad (1)$$

$$AVD(j, k, l)$$
$$= \frac{1}{NP} \sum_{i=1}^{NP} (C(i, j, k, P_{true}) - C(i, j, k, PW_{const})) \quad (2)$$

$$RC(j, k)$$
$$= \frac{100(AV(j, k, PW_{true} - AV(j, k, PW_{const}))}{AV(j, k, PW_{const})} \qquad (3)$$

where

NP	number of clear-sky pixels identified using the CE-CANT algorithm (Cihlar, 1996);
i	= pixel;
j	= AVHRR channel or NDVI;
k	= period (month);
m	= IWV value used.

To examine the effectiveness of various IWV formulations, we prepared several IWV composites from the NCAR data set. They were designed to help determine whether a seasonally variable, but interannually constant, data set could be employed. This would be helpful from the practical perspective since the processing would be considerably easier. The composites were prepared using the following formula:

$$PW(i, k) = F(PW(i, k, y)) \qquad (4)$$

where

i	= pixel (clear sky only);
k	= period;
y	= year;
F	represents the following selection functions:

$$F_{\min 10d} = \text{minimum IWV for } (i, k, 1996);$$
$$F_{avg10d} = \text{average IWV for } (i, k, 1996);$$
$$F_{\min 10y} = \text{minimum IWV for } (i, k, y),$$
$$y \in \langle 1987, 1996 \rangle;$$
$$F_{\min 8y} = \text{minimum IWV for } (i, k, y),$$
$$y \in \langle 1987, 1996 \rangle$$
$$\text{after eliminating the highest and}$$
$$\text{the lowest IWV value};$$
$$F_{avg10y} = \text{average IWV for } (i, k, y),$$
$$y \in \langle 1987, 1996 \rangle;$$
$$F_{avg8y} = \text{average IWV for } (i, k, y),$$
$$y \in \langle 1987, 1996 \rangle$$
$$\text{after eliminating the highest and}$$
$$\text{the lowest IWV value.}$$

Three composite periods were thus considered: the adjacent ten days, ten years, and ten years after eliminating two extreme outliers. It was expected that the first (second) composites would have the best (worst) correspondence to the IWV$_{true}$ data set. The minimum functions were used assuming that clear-sky pixels would likely have lower IWV. The two groups [IWV$_{true}$ and IWV(i, k)] were then compared using regression analysis (Section III-C).

III. RESULTS

A. Effect of IWV on C1, C2, and NDVI Corrections

Fig. 1 shows the effect of IWV on individual AVHRR channels and the NDVI. From the set of 1600 simulation runs, only some combinations were chosen for Fig. 1 to illustrate the trends. These values encompass the reflectance range of most
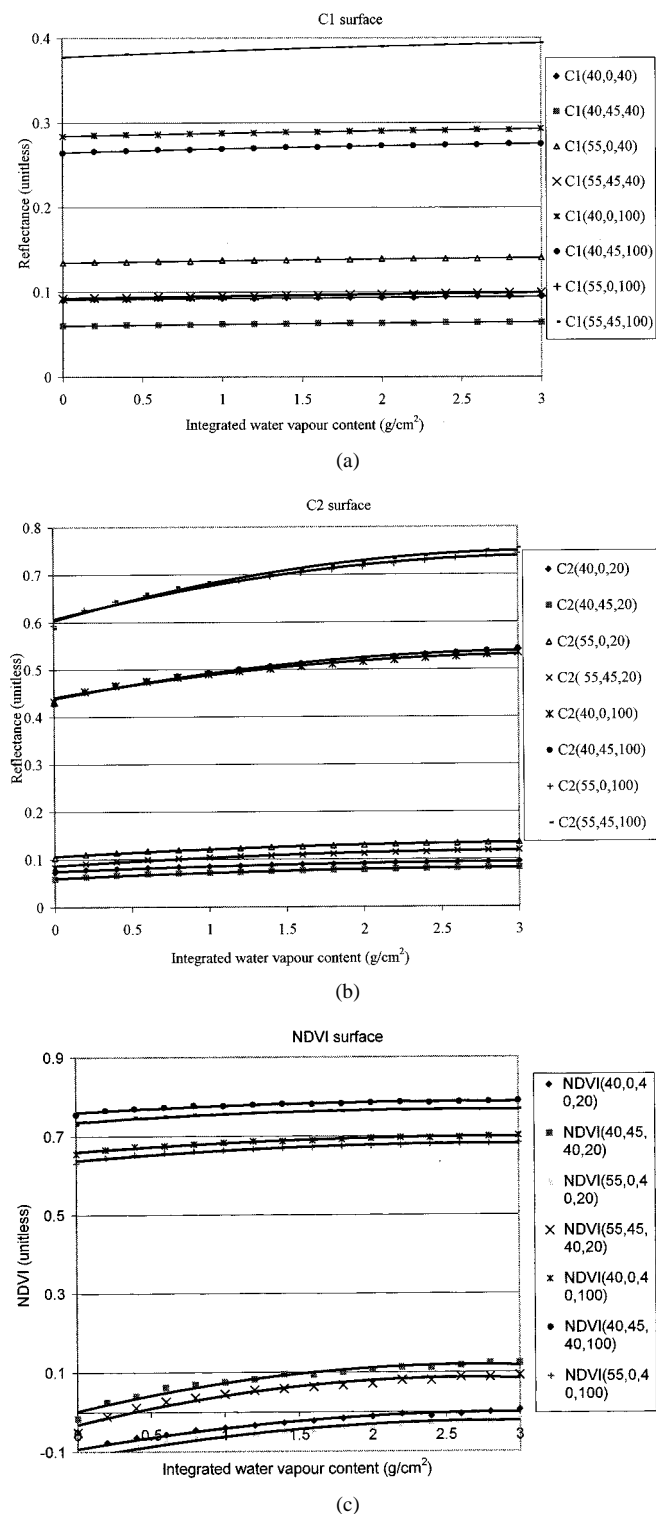
Fig. 1. Effect of IWV on surface values for various combinations solar zenith angle (first number in the legend in degrees), view zenith angle (second number, in degrees), and AVHRR top-of-the-atmosphere radiance (third number, in $Wm^{-2}sr^{-1}$). (a) AVHRR channel 1, (b) channel 2, and (c) NDVI.

term. The nonlinearity of the water vapor effect was higher at SZA $= 55°$ compared to $45°$. The coefficient for the quadratic term also increased by a factor of 1.5 to 3 as the VZA changed from 0 to $45°$. Among all the combinations in Fig. 1(a), the linear term varied by a factor of four (from 0.002 at [SZA $= 40°$, VZA $= 45°$, TOA $= 40$] to 0.008 for [$55°$, $45°$, $100°$]), and the ratio of the quadratic to the linear terms ranged from 0.057 ($40°$, $0°$, $100°$) to 0.111 ($55°$, $0°$, $40°$).

In channel 2, the IWV dependence was more pronounced, especially at higher radiance levels [Fig. 1(b)]. The nonlinearity in the IWV effect was relatively stable among the different combinations, the ratio of the quadratic to the linear term equal to 0.154 ± 0.003. On the other hand, the linear term increased at higher radiance levels by a factor of 4.7 to 6.9. For a given SZA and fixed TOA radiance, the change in VZA had a limited effect at high radiance levels but an appreciable one on low C2 values [Fig. 1(b)]. Thus, C2 values were relatively more sensitive to IWV amounts at high radiance levels, and to the SZA and VZA at low radiance levels.

Since NDVI is calculated as the difference over the sum between C2 and C1, the above trends affect its behavior as well. Overall, NDVI computed from surface reflectance was much more sensitive to IWV at low IWV values [Fig. 1(c)]. In the IWV range $\langle 0, 3.0 \rangle$, NDVI increased more at low NDVIs (~0.1) compared to high NDVI (~0.03), and also appeared more nonlinear at low NDVI values. However, comparing average regression coefficients between the low and high NDVIs in Fig. 1(c), the changes within both linear and nonlinear terms were similar, a factor of approximately 2.9. The apparent nonlinearity is thus a consequence of the NDVI definition, the sensitivity being higher when the difference C2-C1 nears zero. The impact of VZA increase from 0 to $45°$ was similar in absolute terms (~0.1) but again, relatively more significant at low NDVI values. The same is true for SZA dependence, although the absolute change was only 0.02–0.03 as SZA increased from $40°$ to $55°$ [Fig. 1(c)]. Thus, while in absolute magnitude, the nonlinear dependence on IWV is most evident at high C2 values [Fig. 1(b)], the normalizing effect of NDVI shifts the sensitivity to low C2, particularly for terrestrial targets where C2 radiances are higher than for C1 in most cases.

The rate of change in individual values is further characterized in Fig. 2, which shows the slopes of the curves in Fig. 1 as a function of IWV. Overall, the trend is the same for both C1 and C2. With increasing IWV, the sensitivity to IWV diminished in an approximately linear manner. The sensitivity was much greater at higher radiance levels, higher SZAs and higher VZAs. In both C1 and C2, SZA dependence was stronger than that for VZA. However, there was a major difference between the two channels, with C2 sensitivity almost ten times higher [Fig. 2(b) versus (a)]. Furthermore, the C2 slope was much steeper, reaching zero at IWV $\cong 3.2$ g/cm^2, while that for C1 remained positive throughout. The relative importance of VZA was greater for C1 than for C2, as evident at higher radiance levels. C1 slopes also exhibited an interaction between SZA and VZA dependence, evident by the cross-over point at higher IWV values with increasing SZA (e.g., compare the SZA $= 40°$/ VZA $= 0$ or $45°$ with SZA $= 55°$).

terrestrial targets. A second degree polynomial curve was fitted to each data set. For AVHRR channel 1 [Fig. 1(a)] and given a fixed TOA radiance, the surface reflectance increased rather slowly with increasing IWV. The increase was only weakly nonlinear, and the coefficient for the quadratic term was about an order of magnitude lower than that associated with the linear
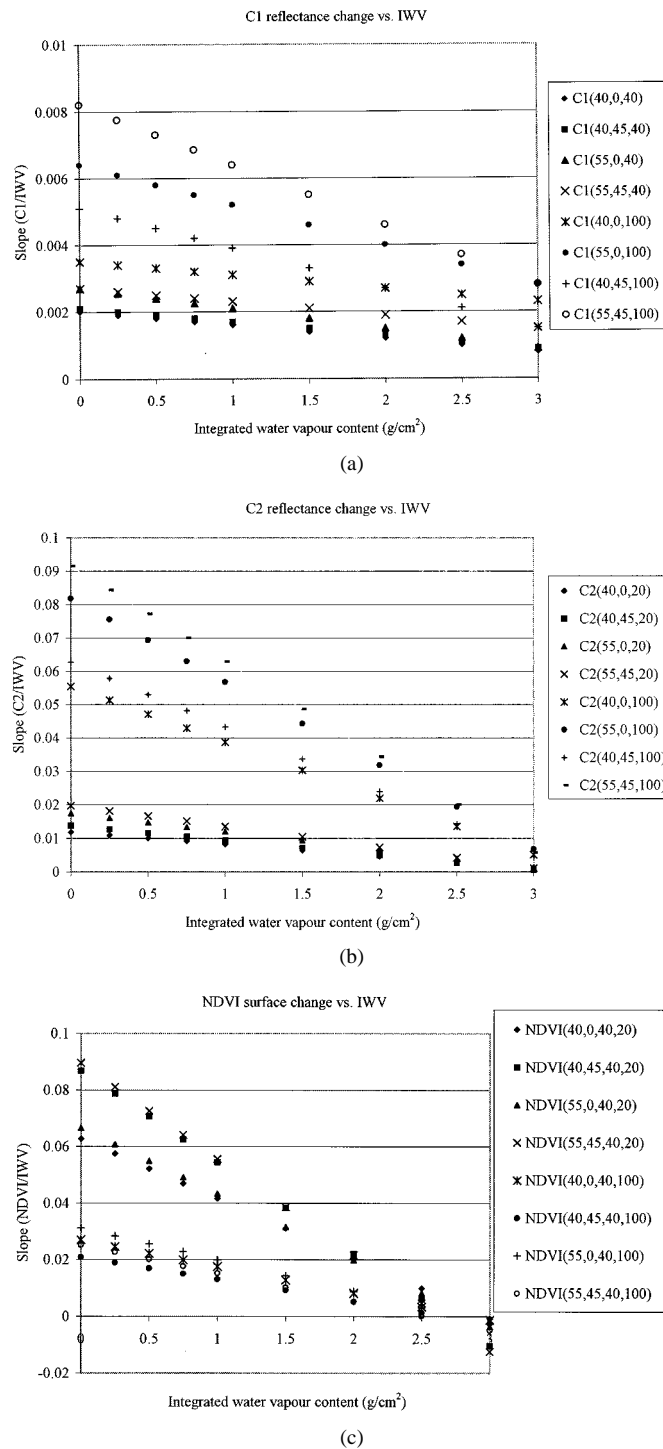
(a)

(b)

(c)

Fig. 2. Sensitivity of surface values derived from AVHRR data to integrated water vapor content IWV, for various combinations solar zenith angle (first number in the legend, in degrees), view zenith angle (second number, in degrees), and AVHRR top-of-the-atmosphere radiance (third number, in $Wm^{-2}sr^{-1}$). (a) AVHRR channel 1, (b) channel 2, and (c) NDVI.

The dissimilar C1 and C2 behavior leads to large differences in the sensitivity of NDVI. At low NDVI and low IWV values, NDVI changes rapidly with increasing IWV [Fig. 2(c)]. At high NDVIs, the sensitivity to IWV changes is about 1/2 or less of that at low NDVI. Note that the curves for low and high NDVI cross at IWV $\cong$ 2.5–3.0 g/cm^2, indicating that the sensitivity of NDVI to IWV is approximately the same here regardless of
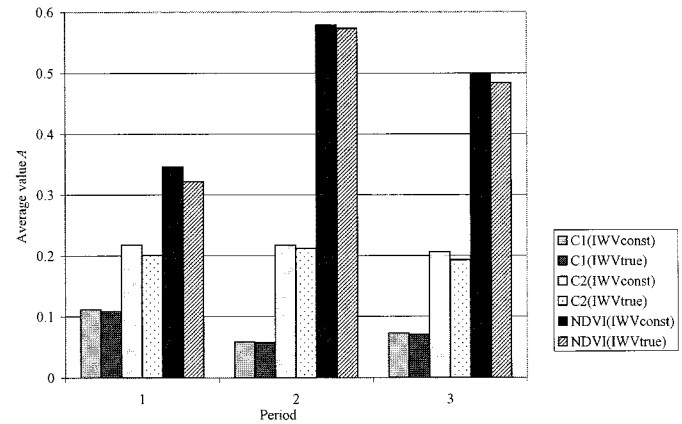

Fig. 3. Average of pixel-by-pixel difference (clear-sky land pixels for Canada) between AVHRR-derived quantities with two integrated water vapor content values for channel 1, channel 2, and NDVI. Periods 1, 2, and 3 represent May 1–10, July 21–31, and October 1–10 in 1996, respectively.

NDVI magnitude. At very high IWV, NDVI slope was negative for all the combinations, indicating decreasing NDVI. However, as shown below, such values are rarely encountered over land at northern latitudes. Fig. 2(c) also clearly shows that for high NDVI values, the differences in sensitivity to various combinations of SZA, VZA, and IWV are greatly diminished compared to low NDVI.

In summary, the above simulations show that in most cases, IWV has greater effect on C2 than on C1 in absolute as well as relative terms. Significant differences exist between the two channels in their sensitivity to various combinations of IWV/SZA/VZA in the nonlinearity of the IWV relationship for various radiance/SZA/VZA combinations, at low NDVI values, and at low IWV values. The sensitivity of C1 and C2 is qualitatively similar but shows large differences in magnitude between the channels and also more subtle variations in the VZA/SZA/IWV interactions. Because of the normalizing effect of NDVI and the typical C1/C2 combinations for terrestrial targets, NDVI is most sensitive to IWV at low IWV and low NDVI values, with VZA and SZA having smaller effect in that order. The above results also show the consequence of choosing a fixed IWV $\cong$ 2.5 g/cm^2 for atmospheric corrections. If the true IWV is smaller and given the same TOA radiance to begin with, both C1 and C2 will be overestimated as will NDVI. The degree of overestimation depends on the difference between the specified and actual IWVs as well as on the particular combination of C1, C2, SZA, and VZA.

B. Impact of Constant IWV on AVHRR Data

Fig. 3 shows the mean values $AV(j, k, l)$ [(1)] for the AVHRR composites obtained for IWV_{const} and IWV_{true} (the latter determined for that pixel on the date of acquisition), considering clear-sky pixels only. In all cases, the new values were smaller than those with a constant IWV. This reflects the fact that the original IWV was too high, thus causing SMAC to overcorrect. The decrease was smallest in July and largest in May. This is to be expected based on Fig. 4, which shows the average precipitable water for all clear-sky pixels for 20 individual ten-day periods in 1996, i.e., $AV(IWV, k, IWV_{true})$.
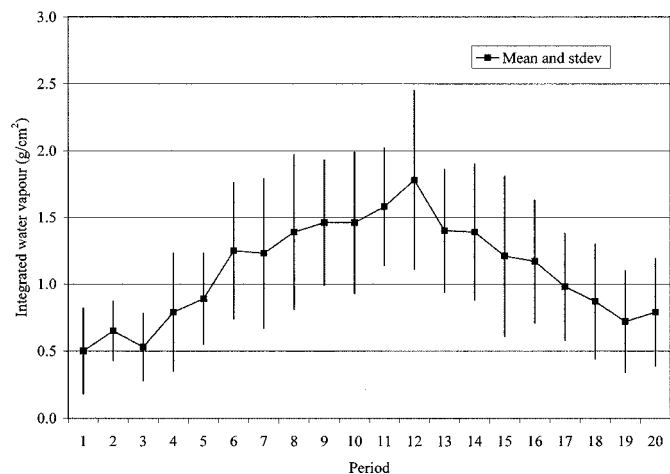
Fig. 4. Average integrated water vapor content for clear-sky pixels in 20 ten-day compositing periods in 1996 for Canadian land mask (clear-sky pixels only). The values were derived on the basis of the NCAR data set.

During the growing season, the average IWV increased from fairly low values in the spring ($\sim$0.6 g/cm^2), reached maximum values in the summer ($\sim$1.7), and decreased more gradually ($\sim$0.8) in the fall. This trend, and particularly the low spring values, were confirmed by detailed measurements during BOREAS [11]. The mean values also differed more for C2 than C1 (Fig. 3), as expected from Fig. 1.

The average surface reflectance difference AVD [(2)] was fairly small for C1: -0.003 in May, -0.001 in July, and -0.002 in October [Fig. 5(a)]. Again, it was much higher for C2, about -0.017, -0.005, and -0.014 for the three periods. The AVD for NDVI was also fairly high in May (-0.024), followed by October (-0.014). To obtain a "typical maximum" value for AVD values, we determined the 10-percentile of the clear-sky pixels for each channel-period combination for data in Fig. 3. This limit was used because most values will be smaller [see (2)]. Results show [Fig. 5(b)] typical upper overestimates of NDVI (up to 0.034), C2 (0.025), and C1 (0.005) by using IWV$_{const}$ during the growing season.

The relative decreases RC after using IWV$_{true}$ [(3), Fig. 5(c)] were especially high for C2: 8.4% in May, 6.6% in October, and 2.4% in July. This was followed by similar decreases in NDVI (7.5% in May, 2.8% in October, but only 0.9% in July). The lower change in NDVI response for October was mostly due to compensating change in C1 [Fig. 5(c)].

The above changes are clearly quite large and are likely to lead to substantial overestimates in biophysical variables based on C2 or indices such as NDVI, especially outside the peak green (mid-summer) period. The constant IWV is therefore not appropriate for atmospheric corrections. In the next section, we explore alternative data sets that might be used for this purpose.

C. Which are the Appropriate IWV Data Sets?

In this study, we assumed that the IWV value for a pixel obtained for the same date as the AVHRR radiance measurement is the most accurate estimate. However, from a data processing viewpoint, this is not an advantageous solution since a distinct IWV data set must be created for each compositing period. In addition, a consistent IWV data series must be available for the
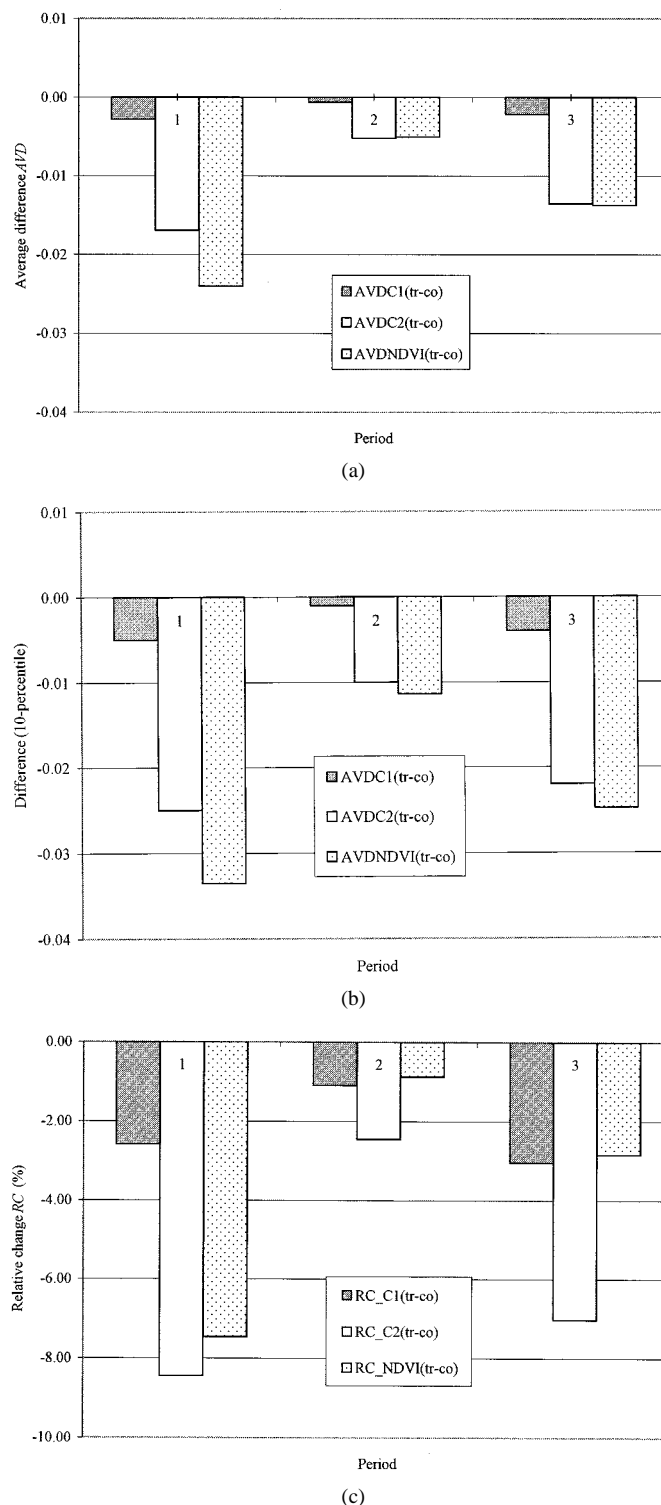

(a)

(b)

(c)

Fig. 5. Effect of different integrated water vapor content values on the pixel-by-pixel difference for clear-sky land pixels of Canada, shown for three periods. Periods 1, 2, and 3 represent the periods May 1–10, July 21–31, and October 1–10 in 1996. (a) average difference AVD, (b) 10-percentile (the value was closer to zero for 90% of the pixels), and (c) relative change RC.
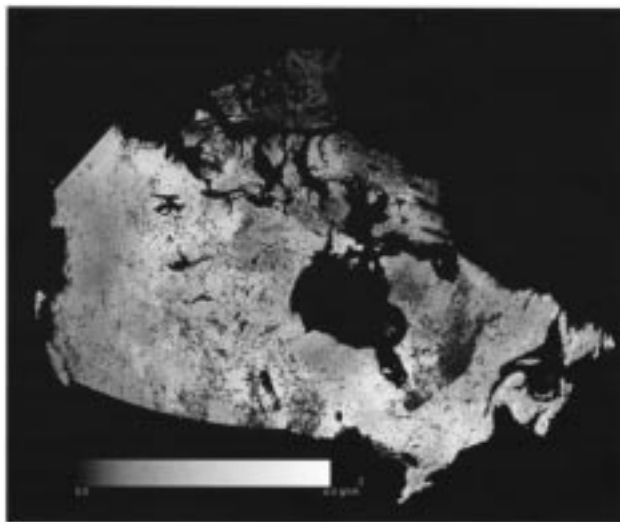
entire period during which AVHRR data are to be corrected, now or in the future. We therefore explored the option of using "climatic" IWV composites which could be pixel- and compositing period-specific, but would not vary from one year to another. To this end, several composites were prepared [(4)] and compared
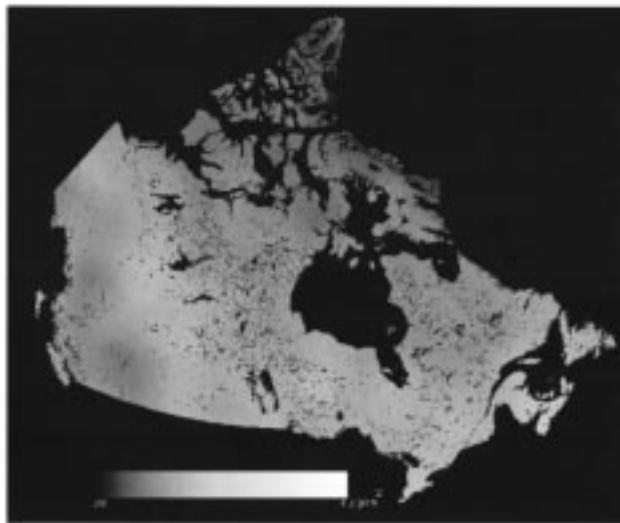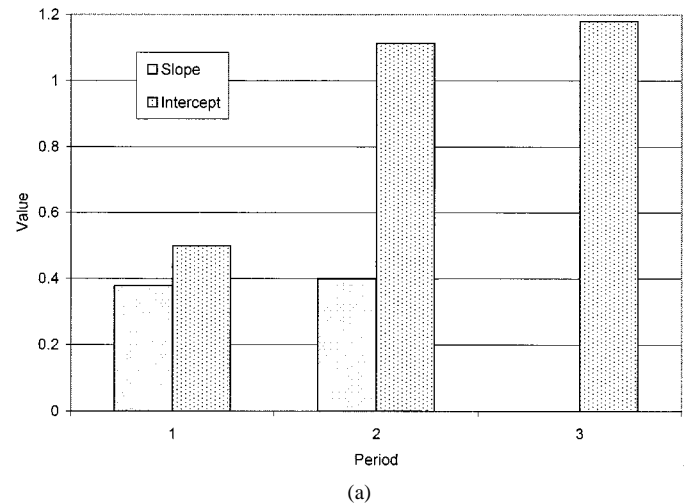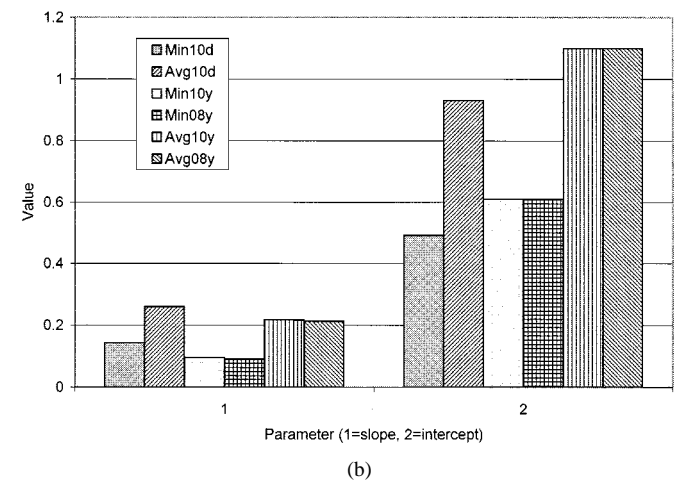
(a)
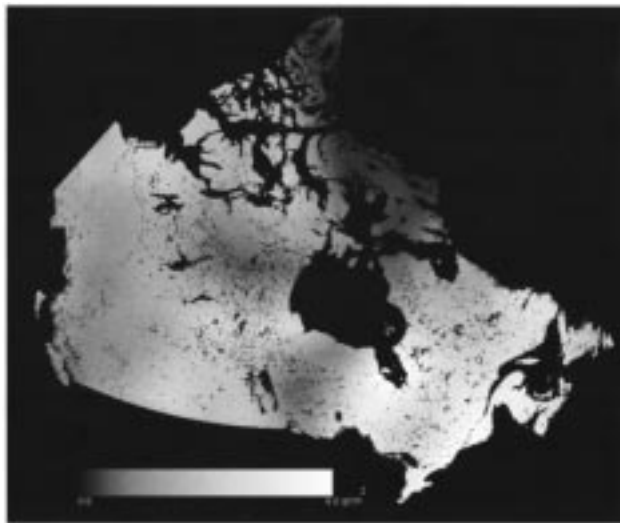
(b)

(c)

Fig. 6. Example of integrated water vapor content data for the Canadian landmass. (a) July 25, 1996, (b) average over the period July 21–31, 1996 (IWV_{avg10d}), and (c) date-specific composite the period July 21–31, 1996 (IWV_{true}).

(a)

(b)

Fig. 7. Slope and intercept of regression lines between integrated water vapor content IWV in two data sets, pixel selection date-specific ($=x$), and a composite over a longer period ($=y$). (a) IWV is an average value for the period during which the AVHRR pixel was selected. Periods 1, 2, and 3 represent May 1–10, July 21–31, and October 1–10 in 1996, respectively. (b) Slopes and intercepts for six composite IWV data sets, prepared for different time periods and compositing criteria. The values represent an average for the three periods in 1996.

to the IWV_{true} composite for each of the three periods. Fig. 6(b) shows an example of a ten-day average composite IWV_{avg10d}, in comparison with a single-date image [Fig. 6(a)] and the acquisition date-specific composite IWV_{true} [Fig. 6(c)].

If IWV_{true} and the IWV_{est} values were identical, a regression equation $\text{IWV}_{est}(i, k, y) = a^*\text{IWV}_{true}(i, k) + b$ would have $a = 1$, $b = 0$, and a standard error of the estimate (SEE) equal to zero. The values of a and b can thus be used to evaluate the representativeness of IWV_{est}. We found that in all cases, the composite data sets IWV_{est} underestimated the true values and furthermore, they distorted the relation between the two by "flattening" the regression. As an example, Fig. 7(a) shows coefficients a and b for IWV_{avg10d} for three periods. In the extreme case (October period), the slope between the two was close to zero. We also found that the composites representing average values were much closer than minimum composites, indicating that clear-sky pixels did not contain significantly less IWV than others. This is evident from Fig. 7(b), which contains average a and b values for the three periods. The slope varied between

TABLE I
EFFECT OF ERROR IN ESTIMATING IWV$_{est}$ FOR CONIFEROUS FOREST COVER

Period in 1996	Mean *IWV* (g/cm^2)	TOA radiance (Wm^{-2}μm^{-1}sr^{-1})		C2 surface reflectance (dimensionless)			NDVI (dimensionless)		
		C1	C2	-SEE	Mean	+SEE	-SEE	Mean	+SEE
May 1-10	0.5	46	44	0.079	0.08	0.08	0.36	0.38	0.39
July 21-31	1.68	24	42	0.191	0.195	0.201	0.77	0.77	0.77
Oct 1-10	0.79	20	22	0.08	0.084	0.086	0.52	0.54	0.56

0.095 and 0.26 and the intercept from 0.49 to 1.1. Thus, the sensitivity to changing IWV was clearly undervalued by IWV$_{est}$ and was compensated for by high intercepts. Note that all minimum-value composites had low intercepts as well, thus consistently underestimating IWV$_{true}$.

Among the IWV$_{est}$ composites tested, the standard error of the estimate (SEE) was about 0.2. However, if these composite were to be used for AVHRR corrections, the relation to be used would have to be IWV$_{est}(i, k) = c^*$IWV$_{test}(i, k, y) + d$. In this case, the standard error of IWV$_{est}$ was found to be about 0.4. Such a value would introduce an additional uncertainty into the corrected AVHRR value. As an example, Table I shows the impact on channel 2 and NDVI for coniferous forest. The TOA radiance data are the mean values for this cover type in the three periods, and the atmospheric corrections were made for the IWV$_{true}$ values corresponding to this cover type and period. The effect varies with season, up to 0.04 for NDVI and SEE = 1.0. Note that this value would double to include 95% of the pixels, and it would also increase for cover types and periods with low NDVIs (Fig. 1). Therefore, the IWV$_{est}$ composites are not a viable substitute for IWV values obtained for each pixel's acquisition date.

IV. DISCUSSION AND CONCLUSIONS

The above analyses demonstrate the importance of the assumed integrated water vapor content on the atmospheric correction of satellite optical data. The effects are greater for the near-infrared channels because of H$_2$O absorption bands located in this region. In addition, at the radiance values and sensing geometries typical for northern terrestrial data sets, the assumed water content interacts with the TOA radiance levels as well as solar and viewing zenith angles to introduce more subtle sources of noise in the computed surface reflectance. Because of these effects and given typical land target values, NDVI is more influenced at low values. For actual data representing the Canadian landmass in 1996 and in comparison with a constant IWV value of 2.3 g/cm^2, the C2 increased by up to 8.4% and NDVI by 7.5% in relative terms. This increase is entirely due to the difference between the actual and assumed IWVs, since all other parameters were kept constant.

From the images of IWV$_{true}$ prepared for the three periods, it is clear that IWV varies seasonally as well as spatially. The extrapolation of a constant summer value would cause greatest errors in the spring because of the relatively dry atmosphere over the boreal region [11]. Furthermore, location-specific composites are needed to account for the latitudinal (and longitudinal) dependence [Fig. 6(a)]. However, even pixel-specific composites obtained for short time periods are not good representations of the IWV values (Fig. 6). The use of such composites would introduce substantial uncertainties into the estimation of surface reflectances and derived indices.

The above findings lead to the conclusion that pixel- and date-specific IWV estimates are necessary for atmospheric corrections of satellite optical measurements at northern latitudes. The only present source of such data are atmospheric model assimilation runs. This raises other issues. The spatial resolution of these models is coarse in comparison with satellite pixel sizes, thus the derived pixel-specific values are approximations at best. The regional averaging effect is also evident in Fig. 7, both for single dates [Fig. 7(a)] and for longer composite periods. Second, consistent assimilation runs are required for the entire period for which satellite data sets are to be corrected. The accuracy of the model estimates can vary [9], although progress in data assimilation is being made and the quality of such data sets will thus continue to improve. Ultimately, the preferred approach will be direct measurement using appropriate spectral channels in new satellite sensors. However, this will not solve the problem with previous data, and since the length of an observation period is a critical requirement for terrestrial studies, the use of ancillary IWV data sets will remain an important data correction strategy in the future.

REFERENCES

[1] J. M. Chen, "Evaluation of vegetation indices and a modified simple ratio for boreal applications," *Can. J. Remote Sensing*, vol. 22, pp. 229–242, 1996.

[2] J. Cihlar, H. Ly, Z. Li, J. Chen, H. Pokrant, and F. Huang, "Multitemporal, multichannel AVHRR data sets for land biosphere studies: artifacts and corrections," *Remote Sens. Environ.*, vol. 60, pp. 35–57, 1997.

[3] J. Cihlar, J. Chen, and Z. Li, "Seasonal AVHRR multichannel data sets and products for studies of surface-atmosphere interactions," *J. Geophys. Res.-Atmos.*, vol. 29, pp. 625–629 640, 1977.

[4] J. Cihlar, J. Chen, Z. Li, F. Huang, R. Latifovic, and R. Dixon, "Can interannual land surface signal be discerned in composite AVHRR data?," *J. Geophys. Res. Atmos.*, pp. 23 163–23 172, 1998.

[5] J. C. Eidenshink and J. L. Faundeen, "The 1 km AVHRR global land data set: First stages in implementation," *Int. J. Remote Sensing*, vol. 15, pp. 3443–3462, 1994.

[6] J. R. Herman, P. K. Bhartia, C. G. Wellemeyer, C. J. Seftor, G. Jaross, B. M. Schlesinger, O. Torres, G. Labow, W. Byerly, S. L. Taylor, T. Swissler, R. P. Cebula, and X.-Y. Gu, "Meteor-3 total ozone mapping spectrometer (TOMS) data products user's guide," NASA, Washington, DC, 1996.

[7] M. E. James and S. N. V. Kalluri, "The pathfinder AVHRR land data set: And improved coarse resolution data set for terrestrial monitoring," *Int. J. Remote Sensing*, vol. 15, pp. 3347–3363, 1994.

[8] C. O. Justice, T. F. Eck, D. Tanre, and B. N. Holben, "The effect of water vapor on the normalized difference vegetation index derived for the Sahelian region form NOAA AVHRR data," *Int. J. Remote Sensing*, vol. 12, pp. 1165–1187, 1991.

[9] E. Kalnay, M. Kanamitsu, R. Kisler, W. Collins, D. Deaven, L. Gandin, M. Iredell, S. Sasha, G. White, J. Woolen, Y. Zhu, M. Chelliah, W. Ebisuzaki, W. Higgins, J. Janowiak, K. C. Mo, C. Ropelewski, J. Wang, A. Leetmaa, R. Reynolds, R. Jenne, and D. Joseph, "The NCEP/NCAR 40-year reanalysis project," *Bull. Amer. Meteorol. Soc.*, vol. 77, pp. 437–471, 1996.

[10] F. X. Kneizys, E. P. Shettle, L. W. Abreau, J. Chetwynd, G. Anderson, W. Gallery, J. Selby, and S. Clough, *User's Guide to LOWTRAN-7, AFGL-TR-88-0177*. Hanscom AFB, MA: Air Force Geophys. Lab., 1988.

[11] B. L. Markham, J. S. Schafer, and B. N. Holben, "Atmospheric aerosol and water vapor characteristics over north central Canada during BOREAS," *J. Geophys. Res. Atmos.*, pp. 29 737–29 745, 1997.

[12] J. V. Martonchik, D. J. Diner, R. A. Kahn, T. P. Ackerman, M. M. Verstraete, B. Pinty, and H. R. Gordon, "Techniques for the retrieval of aerosol properties over land and ocean sign multiangle imaging," *IEEE Trans. Geosci. Remote Sensing*, vol. 36, pp. 1212–1227, 1998.

[13] R. D. McPeters, P. K. Bhartia, A. J. Krueger, J. R. Herman, B. M. Schlesinger, C. G. Wellemeyer, C. J. Seftor, G. Jaross, S. L. Taylor, T. Swissler, O. Torres, G. Labow, W. Byerly, and R. P. Cebula, "Nimbus-7 total ozone mapping spectrometer (TOMS) data products user's guide," NASA Ref. Publ., Washington, DC, 1996.

[14] R. D. McPeters, P. K. Bhartia, A. J. Krueger, J. R. Herman, C. G. Wellemeyer, C. J. Seftor, G. Jaross, O. Torres, L. Moy, G. Labow, W. Byerly, S. L. Taylor, T. Swissler, and R. P. Cebula, "Earth probe total ozone mapping spectrometer (TOMS) data product user's guide," NASA Tech. Publ. 206 895, Washington, DC, 1998.

[15] H. Rahman and G. Dedieu, "SMAC: A simplified method for the atmospheric correction of satellite measurements in the solar spectrum," *Int. J. Remote Sensing*, vol. 15, pp. 123–143, 1994.

[16] R. Richter and W. Luedeker, "Atmospheric water vapor from MOS-B imagery," *Int. J. Remote Sensing*, vol. 20, pp. 1133–1140, 1999.

[17] B. Robertson, A. Erickson, J. Friedel, B. Guindon, T. Fisher, R. Brown, P. Teillet, M. D'Iorio, J. Cihlar, and A. Sancz, "GEOCOMP, A NOAA AVHRR geocoding and compositing system," in *Proc. ISPRS Conf., Commission 2*, Washington, DC, 1992, pp. 223–228.

[18] E. Vermote, D. Tanré, J. L. Deuzè, M. Herman, and J. J. Morcrette, "Second simulation of the satellite signal in the solar spectrum, 6S: An overview," *IEEE Trans. Geosci. Remote Sensing*, vol. 35, pp. 675–686, 1997.

J. Cihlar, photograph and biography not available at the time of publication.

I. Tcherednichenko, photograph and biography not available at the time of publication.

R. Latifovic, photograph and biography not available at the time of publication.

Z. Li, photograph and biography not available at the time of publication.

J. Chen, photograph and biography not available at the time of publication.